

MEDICAL ROBOTICS

An agglutinate magnetic spray transforms inanimate objects into millirobots for biomedical applications

Xiong Yang¹, Wanfeng Shang^{2,3}, Haojian Lu¹, Yanting Liu¹, Liu Yang¹, Rong Tan¹, Xinyu Wu^{3,4*}, Yajing Shen^{1,5*}

Copyright © 2020
The Authors, some
rights reserved;
exclusive licensee
American Association
for the Advancement
of Science. No claim
to original U.S.
Government Works

Millirobots that can adapt to unstructured environments, operate in confined spaces, and interact with a diverse range of objects would be desirable for exploration and biomedical applications. The continued development of millirobots, however, requires simple and scalable fabrication techniques. Here, we propose a minimalist approach to construct millirobots by coating inanimate objects with a composited agglutinate magnetic spray. Our approach enables a variety of one-dimensional (1D), 2D, or 3D objects to be covered with a thin magnetically drivable film (~100 to 250 micrometers in thickness). The film is thin enough to preserve the original size, morphology, and structure of the objects while providing actuation of up to hundreds of times its own weight. Under the actuation of a magnetic field, our millirobots are able to demonstrate a range of locomotive abilities: crawling, walking, and rolling. Moreover, we can reprogram and disintegrate the magnetic film on our millirobots on demand. We leverage these abilities to demonstrate biomedical applications, including catheter navigation and drug delivery.

INTRODUCTION

Insect-scale robots (or millirobots) may find use in biomedical, exploration, and other emerging applications that require distinct controllability, adaptability, safety, and integrity (1–5). Recent progress in materials has enabled smart actuators with different driving mechanisms, such as magnetic fields, biohybrid artificial muscles, photochemical/photothermal effects, shape-memory polymers, etc. (6–9). By introducing biomimetic design (e.g., helix, legged, jellyfish, etc.), those milli-actuators can be formed into millirobots that realize effective locomotion and perform complex tasks in harsh environments (10–14). However, the in-depth interaction between the constructed millirobot and the operated target remains a challenge due to the target's arbitrary size and unstructured shape and unpredictable, limited working space in practice.

Conventionally, traditional robots are designed together with an extra dexterous end effector (15, 16) to interact with the object, e.g., picking, placing, transportation, etc. Limited by energy supply and finite working space, it can be challenging to adopt additional end-effector design to implement tasks at small scale. Nowadays, the usage of soft materials blurs the boundary between robot body and end effector to some extent, allowing a millirobot to be a whole unit for object operation, which greatly reduces the robot's size and enhances flexibility, efficiency, and safety (10, 17, 18). However, to fulfill the in-depth interaction between the millirobot and the unstructured targets at small scale, at least two key challenges must be taken into consideration: unmodifiable structure after fabrication and target size increment. Benefitting from the attributes of soft

materials, such as polydimethylsiloxane (PDMS), Ecoflex, hydrogels, and so on, existing soft millirobots can achieve changeable morphology. However, after fabrication, the inherent structure of the robot is fixed, and its deformability is limited to a few statuses, e.g., compression, stretch, or curl (19). Therefore, it is difficult to design one robot that can adapt to diverse objects with various structures and shapes. Furthermore, even if the millirobot can successfully handle the object, the size increment superposed to the target may be difficult in practice, especially when such operations (e.g., exploration and target delivery) are implemented in a narrow space. These inherent issues essentially challenge the existing materials and robotics, adding more requirements to a coherent robot-object interaction strategy and the corresponding robot design concept in the meantime.

An adhesion strategy could be adapted to most target surfaces irrespective of the specific shape or size of the targets. Recently, scientists have developed diverse adhesive materials and applied them to tissue adhesion and self-healing, as well as engineering applications, such as the instant tough bio tape from the combination of polyvinyl alcohol (PVA) and poly(acrylic acid) (20), the reusable light-melt adhesion by dynamic carbon frameworks in liquid crystal (21), and fast underwater adhesion based on macroscopic supramolecular assembly (22). The progress in adhesive material development and adhering strategy in nature inspires new millirobot designs to achieve the effective robot-object interaction at small scale.

Here, we report a minimalist millirobot construction strategy that transforms inanimate objects into millirobots by coating the target's surface with an agglutinate magnetic spray (M-spray), which consists of PVA, gluten, and iron particles (Fig. 1A). The M-spray can adhere to the surface of a variety of one-dimensional (1D), 2D, or 3D objects, and the covered film (~100 to 250 μm) is thin enough to preserve the target's original size, morphology, and structure. Under the actuation of magnetic field, the constructed millirobots are able to demonstrate a range of locomotive abilities: crawling, walking, and rolling. Our approach offers a general on-demand robot construction method by leveraging the structure and

¹Department of Biomedical Engineering, City University of Hong Kong, Hong Kong SAR 999017, China. ²CAS Key Laboratory of Human-Machine Intelligence-Synergy Systems, Shenzhen Institutes of Advanced Technology, Chinese Academy of Sciences, Shenzhen 518055, China. ³Guangdong Provincial Key Laboratory of Robotics and Intelligent System, Shenzhen Institutes of Advanced Technology, Chinese Academy of Sciences, Shenzhen 518055, China. ⁴SIAT Branch, Shenzhen Institute of Artificial Intelligence and Robotics for Society, Shenzhen 518129, China. ⁵City University of Hong Kong Shenzhen Research Institute, Shenzhen 518057, China.

*Corresponding author. Email: xy.wu@siat.ac.cn (X.W.); yajishen@cityu.edu.hk (Y.S.)

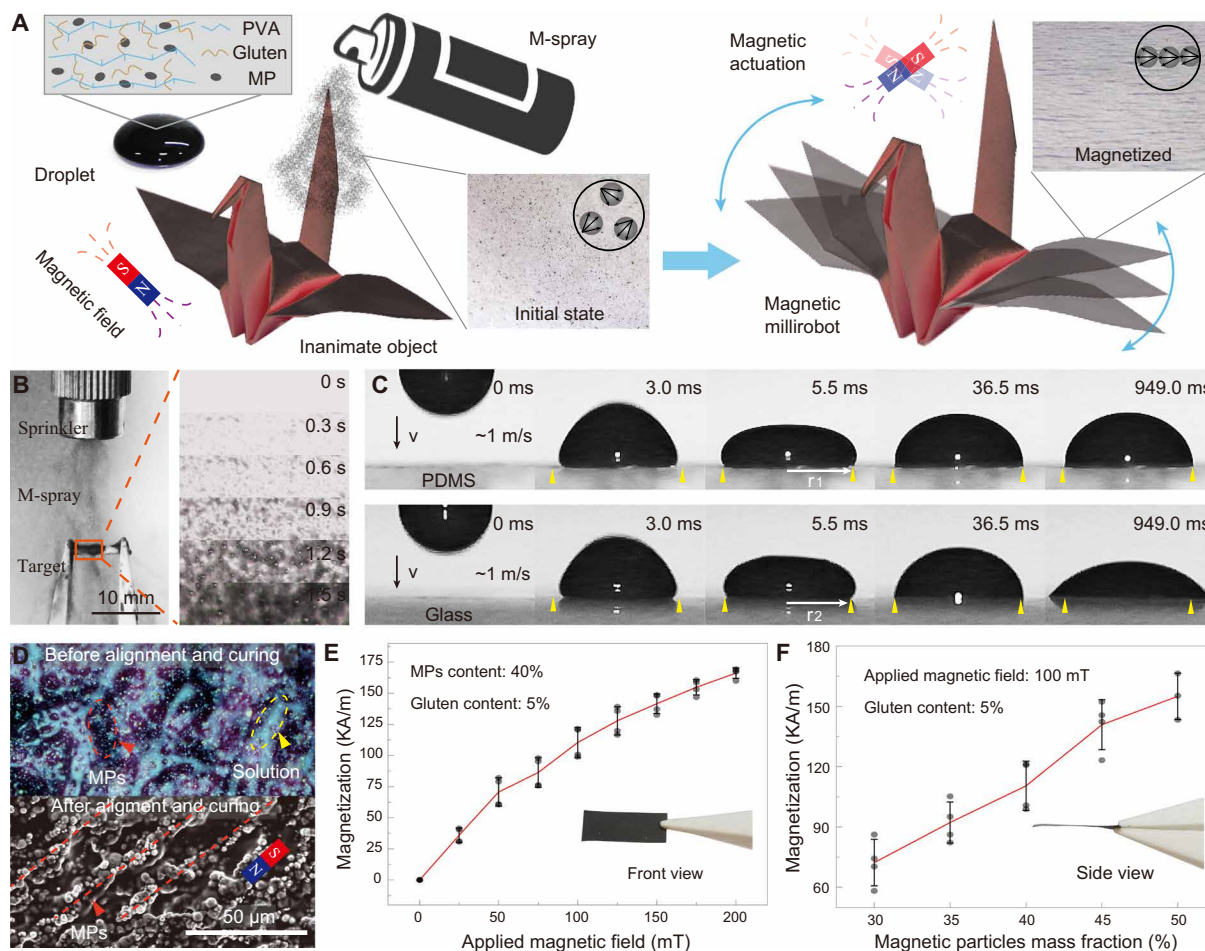


Fig. 1. Agglutinate M-spray converts inanimate objects to millirobots. (A) Schematic of M-spray turning an origami crane into a magnetic millirobot. (B) Coating of M-spray from a pressurized watering can. (C) The adhesion process of M-spray droplets on PDMS and glass surface. Droplets adhere to the substrate stably and firmly without bounce or lateral migration. (D) Surface texture of M-skin before and after alignment and curing. (E) The magnetic susceptibility of the cured M-skin with 40% MPs when the applied magnetic field strength is from 0 to 200 mT. (F) The magnetic susceptibility of the cured M-skin corresponding to various MP content from 30 to 50% under 100 mT. Error bars indicate the SD for $n = 4$ measurements at each data point.

morphology of the targeted objects themselves and may find a wide range of applications in biomedical engineering.

RESULTS

Agglutinate M-spray composition and characterization

The raw material for M-spray is composed by doping gluten and magnetic particles (MPs) into a 10 weight % (wt %) PVA solution with a mass ratio of 1:8:11 at room temperature. Then, the composed material is atomized into droplets and coated on the surface of target object at a speed of ~ 1 m/s, and a thin colloidal-like film (~ 500 μm) is formed as the merging of droplets in a few seconds (Fig. 1B). As illustrated in Fig. 1C, the M-spray droplet can adhere to the substrates immediately. Furthermore, we do not observe any spray recoil—this is distinct from what is observed with a water droplet (fig. S1A). Moreover, after the M-spray lands on the substrate, the radius of the contact area r continuously increases or remains stable but never decreases due to its high agglutination and viscosity. For instance, the contact area of M-spray droplet remains stable on the hydrophobic PDMS surface and increases 56% in ~ 1 s

on the hydrophilic glass surface (Fig. 1C). To further evaluate the wetting ability of M-spray, we conducted control experiments on different substrates—including PDMS, glass, paper, plastic, and wood—several times (fig. S1B and movie S1). The results indicate that the M-spray can achieve a similar contact angle as a water droplet on the hydrophilic surface and a smaller contact angle on the hydrophobic surface, suggesting its high wetting ability to diverse materials. The attributes of high agglutination and viscosity (~ 550 mPa·s), as well as wetting ability, make the M-spray stick on various surfaces stably and firmly, which ensures effective adhesion-based robotization of the inanimate targets.

To endow the controllable actuation, we aligned the random MPs inside the M-spray into orientated chains by applying a ~ 100 -mT directional magnetic field, in which the formed magnetic chains tend to coincide with the magnetic field lines. After thermal curing, a thinner, solidified magnetic film (~ 100 to 250 μm) with oriented easy magnetization axis is obtained on the surface of the inanimate object in several minutes, named magnetic skin (M-skin) for short (Fig. 1D and fig. S2). To quantitatively evaluate its magnetic property, we peeled off the M-skin (10 mm by 10 mm by 0.2 mm) from the

substrate carefully and then characterized its magnetization (Fig. 1, E and F). The results indicate that the M-skin with 40% MPs mass fraction exhibited nearly linear magnetization from 0 to 166.1 kA/m as the applied magnetic field increased from 0 to 200 mT. In addition, the magnetization also almost linearly increased corresponding to the increment of MP mass fraction from 30 to 50% while keeping the applied magnetic field at 100 mT. This directional and controllable actuating capability of M-skin (fig. S3) makes it possible to turn inanimate objects into magnetic millirobots.

The self-adhesive ability of the M-spray is endowed by the component of PVA and gluten. As illustrated in Fig. 2A, before curing, the hydroxyl groups in the molecular chain of PVA combine with water molecules, leading to strong hydrogen bonds ($\sim\text{CH}_2\text{-CH-OH}\cdots\text{H-O-H}\cdots\text{HO-CH-CH}_2\sim$) and a form of viscous high polymer paste. When the paste fills the gap and fully contacts with the surface of target object, they adhere together by van der Waals force (23). On the contrary, after the M-spray is cured to the M-skin, it converts to a solid form, and the strong hydrogen bonds between PVA chains and water are replaced by the weak hydrogen bonds between PVA chains (24). Meanwhile, the van der Waals force between the cured M-spray and other objects becomes negligible due to the poor contact area at the rigid form. As a result, the M-skin can stably adhere to a target object and remain nonviscous to other objects after curing. Specifically, for objects with a rough surface, the generated paste can diffuse into the micropores and remain as a residue when peeling off, where the adhesion will be enhanced by

the hydrogen bonds between the molecular chains of PVA during material tearing (Fig. 2, B and C). In the above process, gluten plays two notable roles in making the cured M-skin reliable: One is to enhance the mechanical property of the structure (fig. S4B), and the other is to increase the adhesive ability (25) on the substrate with a rough surface (fig. S4D). Compared with PVA, the molecular chain of gluten can form a tight network when absorbing water, allowing the cured M-skin to maintain a strong skeleton. However, note that the addition of gluten is not unlimited because a larger ration of gluten will increase the chance of agglomeration in the M-spray atomization and eventually result in failure fabrication. In our work, we chose the ratio of gluten to 5% based on experimental trials.

To demonstrate the adhesive ability of the M-spray, we coated the M-spray between two paper belts (contact area, 5 mm by 5 mm) and then separated them with a constant speed of ~ 1 mm/s (fig. S4E). The experimental result indicates that the M-spray is able to bond the paper belts together with an adhesion strength of ~ 0.17 N/mm² after curing. This value is about 125% of the value obtained with carbon conductive double-faced adhesive tapes (731, carbon tape, 5 mm in diameter, Nisshin EM Co. Ltd.) under the same experimental conditions. As shown in the quantitative peeling-off results presented in Fig. 2D, the average peeling strength of M-spray to different tested materials ranged from 2.8 to 117.2 N/m by case. The adhesion strength to the rough surface is dozens of times stronger than that to the smooth surface, which is mainly caused by the larger bonding force of hydrogen bonds than the van der Waals force as discussed above.

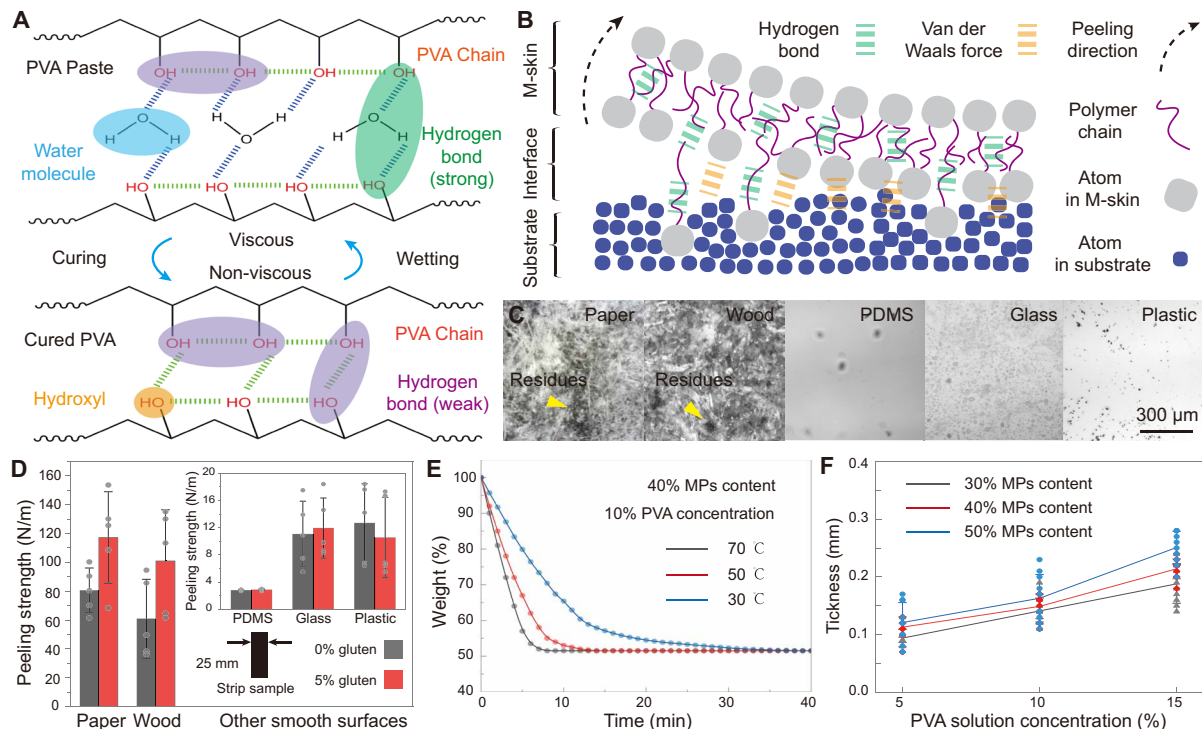


Fig. 2. Self-adhesiveness and adaptiveness of M-spray. (A) The state change of M-spray between viscous and nonviscous forms. (B) Schematic of the bonding force between cured M-skin and substrate surface during the peeling process. (C) Optical microscopy images of the contact surface on testing materials after the M-skin is peeled off. (D) The quantitative peeling strength of M-skin to rough (paper and wood) and smooth surfaces (PDMS, glass, and plastic). Error bars indicate the SD for $n = 5$ measurements at each data point. (E) The curing rate of M-spray at different environment temperatures. (F) Effect of MP content and PVA solution concentration to the final thickness of M-skin. Error bars indicate the SD for $n = 10$.

To further understand the paste-solid transition of M-spray, we investigated the effects of temperature, MP content, and PVA solution concentration on the curing process by contrast experiments. Figure 2E presents the weight change of the M-spray with 40% MP content in the curing process, indicating that higher temperature would greatly speed up the paste-solid transition process. Here, the transition time shortened from ~30 min at 30°C to ~5 min at 70°C due to the faster water evaporation. We also find that the final structure and size of the M-skin is not relevant to the curing speed, suggesting that a faster on-demand construction is achievable by accelerating the paste-solid transition, such as higher temperature, lower humidity, or enhanced air convection. On the other hand, we find that the thickness of M-skin is relevant to the MP content and PVA solution concentration (Fig. 2F). Particularly, it decreases nearly threefold (from 251 to 94 μm) when the MP content decreases from 50 to 30% and the PVA solution concentration varies from 15 to 5%, which could provide guidance for adjusting the M-skin's thickness.

Principle of turning inanimate objects into millirobots

The roboticization of inanimate objects is realized by the directional magnetization of M-skin and the controllable actuation magnetic field. For an inanimate object with a soft or deformable structure, we arrange the easy magnetization axis of M-skin perpendicularly to the deformation direction to achieve a repeatable morphological change (fig. S5A). On the other hand, for a rigid or nondeformable inanimate object, we align the easy magnetization axis of M-skin parallel to its long axis for holistic locomotion, such as slipping, flipping, and rolling (fig. S5B). Theoretically, given a constructed M-skin millirobot with an arbitrary structure, it can be modeled as M parts and N contact lines (or points) with the ground. When the magnetic field is applied or removed away, the motion of the i th single anchor is reliable if the criterion meets $\mathbf{F}_{in} + {}^{i+1}\mathbf{F}_x - {}^{i-1}\mathbf{F}_x + {}^{i-1}\mathbf{F}_z + m_i \mathbf{g} - {}^{i+1}\mathbf{F}_z - \mathbf{F}_{Nn} - \mathbf{F}_{zi} = m_i \mathbf{a} \neq 0$ or $\mathbf{T}_{yi} + {}^{i-1}\mathbf{T}_y - {}^{i+1}\mathbf{T}_y - (\mu \sin \theta_i \cos \theta_i) \mathbf{F}_{Nn} r_i = J \dot{\theta}_i \neq 0$, where $r_i (i = 1, \dots, M)$ is the distance between contact line c_n and mass center m_i of the i th part of robot; μ is friction coefficient; θ_i is the angle between line $c_n - m_i$ and horizontal direction; $\mathbf{F}_{Nn}, \mathbf{F}_{fn}$ are the supporting force and friction force from the ground; and $\mathbf{T}_{yi}, \mathbf{F}_{xi}, \mathbf{F}_{zi}$ are the magnetic moment and pulling forces along the $y, x,$ and z axes, respectively. ${}^{i-1}\mathbf{T}_y, {}^{i-1}\mathbf{F}_x, {}^{i-1}\mathbf{F}_z$ are the equivalent moments to m_i and forces exerted by m_{i-1} part, and ${}^{i+1}\mathbf{T}_y, {}^{i+1}\mathbf{F}_x, {}^{i+1}\mathbf{F}_z$ are the equivalent moments to m_i and forces exerted by m_{i+1} part, respectively (Fig. 3A). In other words, when there exists at least one value i that satisfies the above criteria, the designed M-skin millirobot will respond to the magnetic field, i.e., $\mathbf{a}_i \neq 0$ indicates translation, and $\dot{\theta}_i \neq 0$ indicates swing or rotation.

To explain the above model and exhibit the versatility of M-spray in turning diverse objects into millirobots, we demonstrate the process of converting cotton rope (line), origami (flat), PDMS (curve), and plastic pipe (round) into soft reptile robot, multiple-joint robot, walking robot, and rolling robot, respectively (Fig. 3B and movie S2) (26, 27). The fabrication of these millirobots follows the similar coating, magnetization, and curing process as the M-skin, except for peeling off. Specifically, for the robot with more than one coating area, such as the multi-foot origami robot, a mask is used to protect the unselected region and guarantee accuracy. The detailed fabrication process of these robots is given in Materials and Methods and illustrated in fig. S6. The actuation of these millirobots is

realized by a portable permanent magnet (50 mm by 50 mm by 25 mm) underneath (40 mm), which could generate a magnetic field with a strength of ~50 mT and a gradient of ~1000 mT/m. For the deformable soft reptile robot, the applied swing magnetic field is generated by the reciprocating motion of permanent magnet in the xy plane. With the cooperation of the magnetic pulling force, the constructed reptile robot can creep forward by sliding its two contact points alternately (figs. S5C, S7A, and S8A). For the multi-foot origami robot, the permanent magnet moves up and down in the xz plane to achieve curling and stretching of the robot; by repeating, the robot can crawl like a multi-foot insect (figs. S5D, S7B, and S8B). For the walking robot, the permanent magnet moves in the xz plane with an O trajectory, moving the robot forward in an inchworm-like locomotion style (figs. S5E, S7C, and S8C). For the nondeformable plastic pipe, the magnetic force provides the power for rolling, and the magnetic torque steers the rolling direction (figs. S5F, S7D, and S8D). These results indicate that diverse millirobots can be constructed with different attributes just by following the similar standardized M-spray adhesion process, offering an effective on-demand millirobot construction strategy to fulfill tasks with different environments, surface conditions, and obstacles. More detailed locomotion demonstration, modeling, and analysis of each millirobot are given in Supplementary Text (figs. S9 and S10, table S1, and movie S3).

The strategy of turning inanimate objects into M-skin millirobots fully uses the structure of the objects, leading to several advantages in adaptivity, miniaturization, and efficiency. As the comparison curves show in Fig. 3C, the deformation and locomotion of M-skin millirobot are regulated by the strength and direction of magnetic field, the objects' material property, and inherent structure. Due to the efficient utilization of the target structure, an inanimate target can be actuated by using a small amount of M-spray with a negligible size increment to the object, which can be as low as 1 per mil in volume. Moreover, because most of the applied magnetic energy contributes to the actuation of the target and very little energy is needed to maintain the M-skin itself, the proposed M-spray has an ultrahigh transportation ability of up to several hundred times its own weight. For instance, 0.01 g of M-spray (after curing) can drive a bulk plastic tube with a weight of 3.63 g under normal-level magnetic field (strength, ~50 mT and gradient, ~1000 mT/m), which is ~360 times its own weight and ~1600 times its own volume (fig. S8D). The advantages of M-skin millirobot in high adaptability, negligible size variation, and high working efficiency offer a unique strategy for robot-object interaction at small scales, especially for tasks with limited space.

Topology order reprogramming

The M-skin is also reprogrammable by adjusting the topology order of the MPs without changing the main structure. Under the drying condition, the MPs inside the M-skin are constrained firmly by PVA and gluten, resulting in holistic deformation and locomotion capabilities when external magnetic force or torque is applied. On the other hand, when the M-skin is thoroughly wetted, the spacing between MPs will increase due to PVA swelling, and the constraints to MPs from the PVA and gluten will greatly decrease (Fig. 4A). The MPs inside M-skin can be realigned along the direction of magnetic flux and overcome the constrain when a strong magnetic field is applied.

To intuitively show the reprogramming process, we prepared an M-skin with a low MP mass fraction of 1% for demonstration

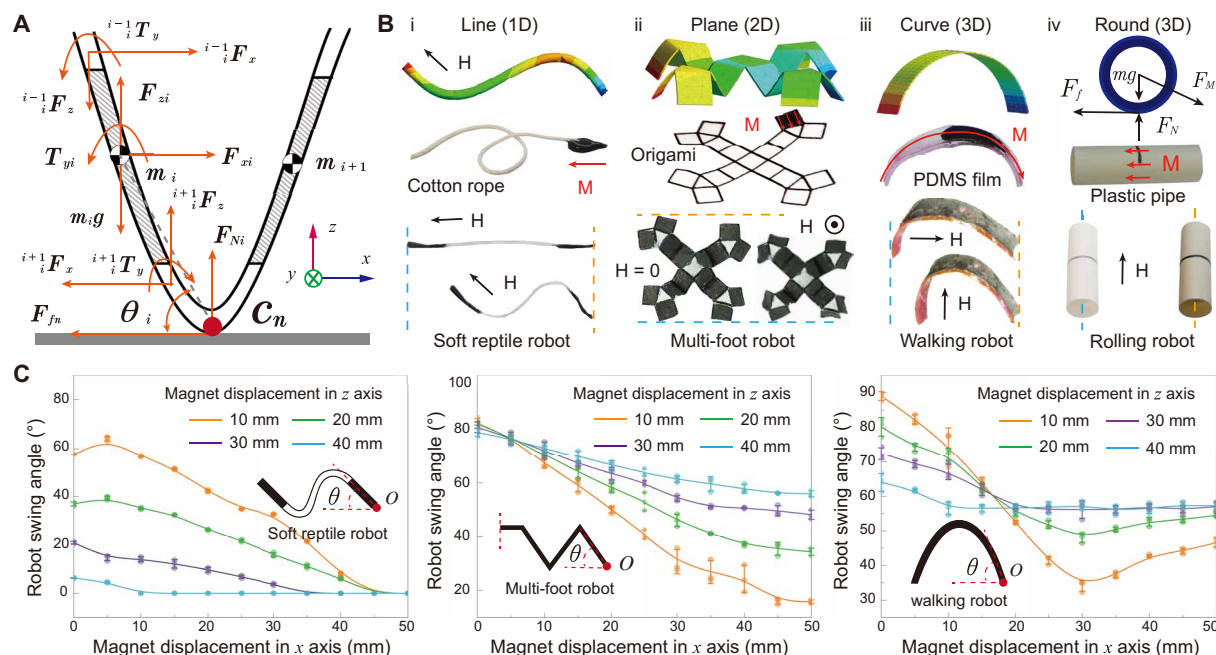


Fig. 3. Principle of turning inanimate objects into millirobots with negligible size variation. (A) The enlarged part of the robot's single anchor for general mechanical analysis. θ_i is the angle between line C_n - m_i and horizontal direction; F_{Ni} , F_{fi} are the supporting force and friction force from the ground; and T_{yi} , F_{xi} , F_{zi} are the magnetic moment and pulling forces along the y , x , and z axes, respectively. ${}^{i-1}T_y$, ${}^{i-1}F_x$, ${}^{i-1}F_z$ are the equivalent moments to m_i and forces exerted by m_{i-1} part, and ${}^{i+1}T_y$, ${}^{i+1}F_x$, ${}^{i+1}F_z$ are the equivalent moments to m_i and forces exerted by m_{i+1} part, respectively. (B) Diverse millirobots from inanimate objects by M-spray coating with negligible size variant, including soft cotton rope (line), origami (plane), PDMS film (curve), and plastic pipe (round). mg is the gravity, and F_N , F_f , F_M are the supporting force, friction force, and magnetic force, respectively. (C) Comparison curves show that the deformation and the locomotion of M-skin millirobots are regulated by the strength and the direction of magnetic field and the substrate's material property and inherent structure. Error bars indicate the SD for $n = 3$.

(Fig. 4B). Here, the M-skin's easy magnetization axis is initially aligned and fixed along the horizontal. Then, we wet it fully and applied an external 200-mT magnetic field perpendicular to the initial magnetization direction. As a result, the easy magnetization axis of the M-skin was turned 90° in 10 min (Supplementary Text and movie S4).

In practice, the reprogramming of the easy magnetization axis in the M-skin with 40% MP mass friction can always be ensured in 5 min as long as the magnetic field strength is sufficient, i.e., larger than 200 mT, based on our experiment trials (Fig. 4C). The results also indicate that the reprogramming efficiency is positively proportional to the applied magnetic field strength. For instance, it takes ~ 5 min to reprogram the direction of easy magnetization axis from horizontal to vertical under a 200-mT magnetic field, and this process is extended to ~ 17 min under a 100-mT magnetic field. Note that the magnetic field for actuation (~ 50 mT) is much lower than the strength for easy magnetization axis reprogramming (200 mT); thereby, the robot constructed by M-skin can keep stable and locomote effectively at the wet or liquid environment, as evidenced by the jellyfish robot in fig. S11. To quantitatively evaluate the efficiency and stability of the easy magnetization axis after realignment, we then conduct contrast experiments to measure the magnetization of M-skin before and after reprogramming. As the results show in Fig. 4D, after reprogramming under a 200-mT magnetic field for 10 min, the magnetization of all the three M-skins exhibited a small discrepancy (13.0, 6.8, and 9.2 kA/m under 200 mT) compared with their initial states, i.e., discrepancy of 7.7, 3.9, and 5.4% for samples

1, 2, and 3, respectively. These results suggest that the proposed reprogramming strategy is feasible and repeatable for rearranging the easy magnetization axis of M-skin.

The on-demand reprogramming ability endows an M-skin millirobot with high adaptivity to achieve diverse locomotions. To demonstrate this, we constructed a simple reptile millirobot (28) by coating M-spray on three sections of a plastic belt (Fig. 4E). Initially, the easy magnetization axes of these three M-skins are aligned along the horizontal. When a swing magnetic field is applied, the M-skins will tilt up or down, and the robot crawls forward by alternating the front anchor and rear anchor like a caterpillar. On the other hand, after the easy magnetization axes are reprogrammed along the diagonal, the millirobot can shrink to an "S" form under a horizontal magnetic field and restore when removing the magnetic field. By repeatedly applying and withdrawing the magnetic field, the millirobot deforms like a concertina to move forward by alternating anchors. Further quantitative analyses reveal that the millirobot with the same structure can exhibit essentially different locomotion styles in deformation angle (Fig. 4F), step size (Fig. 4G), and height variation (Fig. 4H) by reprogramming. Benefiting from the on-demand reprogramming ability, the M-skin millirobot can switch its motion between 3D caterpillar and 2D concertina to adapt to different environments, such as moving with a high speed by caterpillar motion (~ 10 -fold faster than concertina motion) at free space and clinging to the ground by concertina motion for crossing a narrow crevice (interval, ~ 2 mm) (Fig. 4E). More details about the locomotion analysis can be found in Supplementary Text.

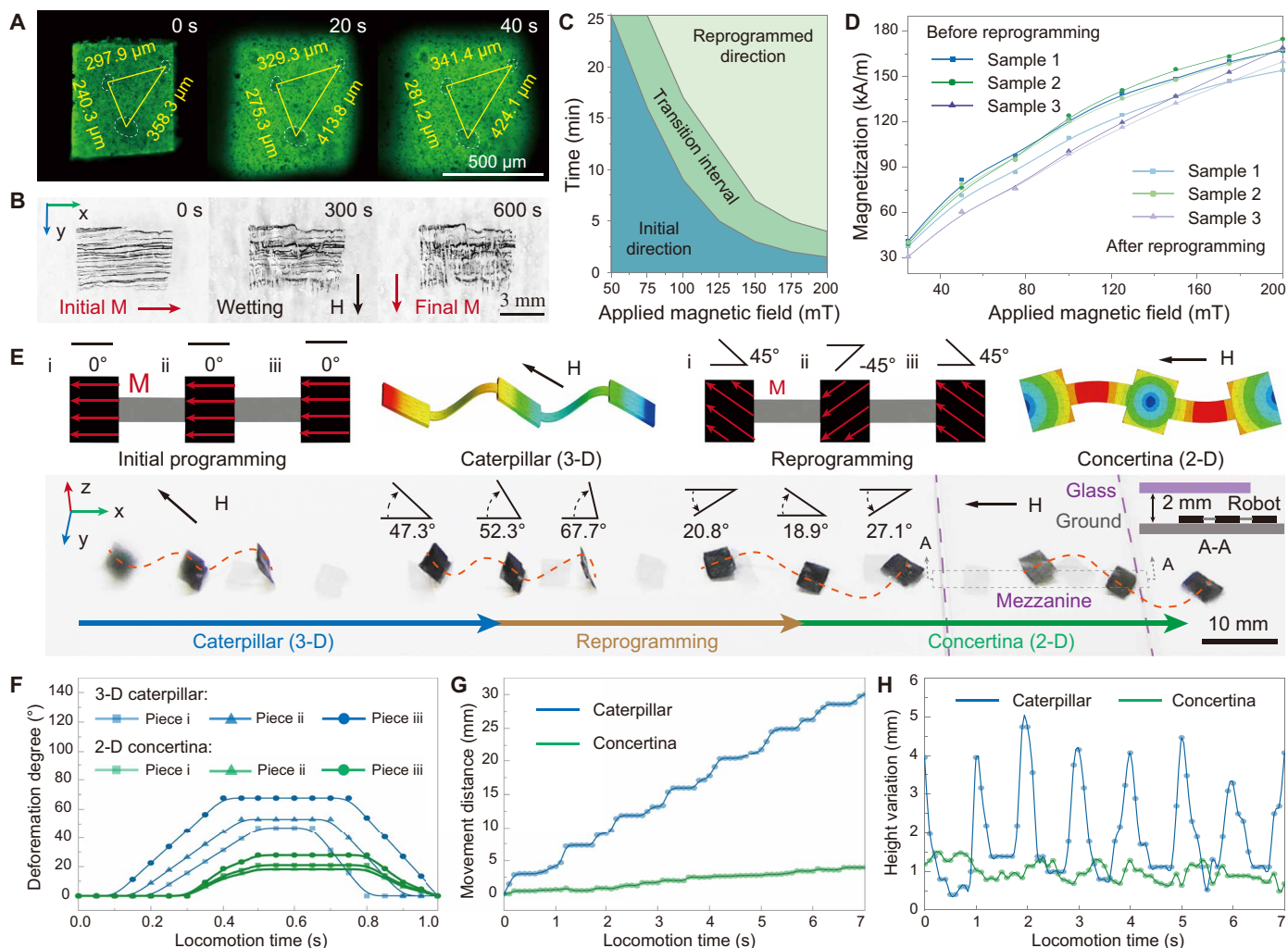


Fig. 4. Topology order reprogramming of M-skin millirobot. (A) Fluorescent photos show the swelling of M-skin under wetting. (B) The reprogramming of cured M-skin’s easy magnetization axis from horizontal to vertical under wetting and a 200-mT magnetic field, during which the demonstrated sample with a MP content of 1% shows the reorganization process. (C) The direction changing state of easy magnetization axis and the corresponding applied magnetic field and reprogramming time. (D) The quantitative magnetization measurement of M-skin before and after reprogramming. The tested sample with a MP content of 40% and a size of 5 mm by 5 mm was reprogrammed under 200 mT within 10 min. (E) The three-section reptile robot demonstrates caterpillar (3D) and concertina (2D) motion before and after reprogramming without structure changing. (F) The deformation of robot during 3D caterpillar and 2D concertina motion, respectively. (G) Step size comparison between caterpillar (3D) and concertina (2D) motion under the same magnetic field strength with a frequency of 1 Hz. (H) Robot height variation as time changes during caterpillar (3D) and concertina (2D) motion.

Magnetic-induced disintegration

The cured M-skin has good stability in still water or under a static magnetic field due to the low solubility of PVA at normal temperature (fig. S12A), which means that an M-skin millirobot can remain stable in an aqueous environment. However, we can controllably disintegrate it by increasing the kinetic energy of MPs to overcome the inner constraints via applying an oscillating magnetic field in an aqueous environment (Fig. 5A and fig. S12B). As shown in Fig. 5B, the disintegrated speed of M-skin is positively proportional to oscillating frequency f from 0 to 3 Hz, and the disintegration can be completed within 4 min under a 10-mT magnetic field with a frequency of 1 Hz. Note that the disintegration time will take several-fold longer after M-skin adheres to objects because the joint surface can enhance its structural integrity (Fig. 5C and fig. S13). The optical images in Fig. 5D display the shedding and disintegration of

M-skin from the multi-foot origami robot under the aqueous environment, where a 10-mT oscillation magnetic field with a frequency of 1 Hz was applied. Although the existing millirobot provides opportunities for effective cargo transportation, the postprocessing of the robot after task remains a big challenge, which may still cause unpredicted side effects. Magnetic-induced disintegration ensures that the constructed M-skin millirobot can disintegrate on command (figs. S11C and S13C and movie S5), making it suitable for controllable cargo unloading. Moreover, the component of MPs is pure Fe in our M-skin design. As a natural metal (ferritin) in the human body, the side effect from its disintegration is negligible (29), making it a good candidate for biomedical applications.

To further understand the disintegration process, we also evaluate the effect of mass fraction and pH value on the disintegration speed. Because gluten can enhance the mechanical property of an

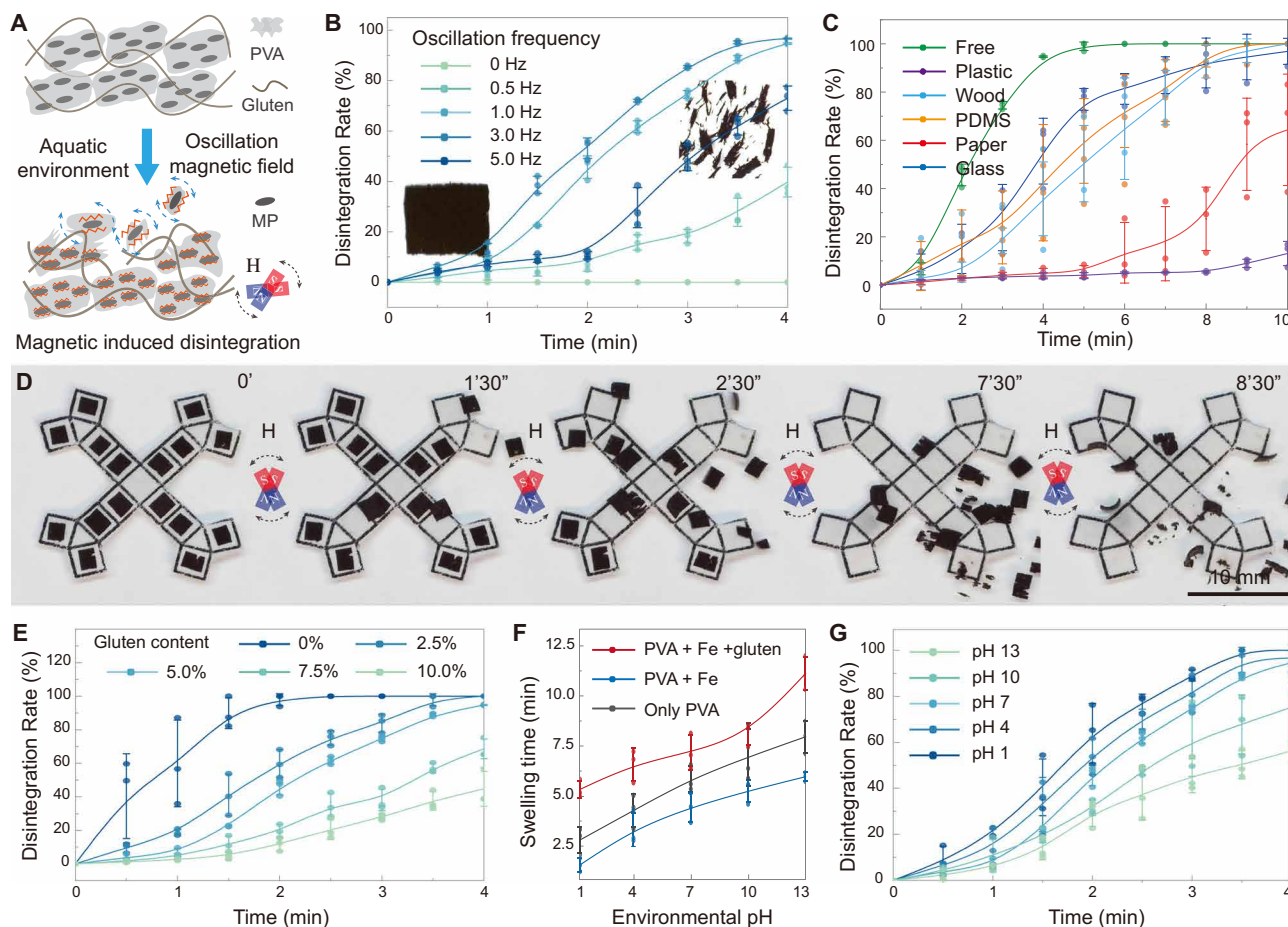


Fig. 5. The magnetic-induced disintegration ability of M-skin. (A) Schematic of the oscillation magnetic-induced disintegration of M-skin in aquatic environment. (B) Free M-skin disintegration rate over time. In this embodiment, the size of cured M-skin is 5 mm by 5 mm, and we applied a 10-mT oscillating magnetic field with a frequency from 0 to 5 Hz. (C) M-skin disintegration rate over time on different materials' surfaces under the oscillating magnetic field with a strength of 10 mT and a frequency of 1 Hz. (D) Photo images depict the shedding and disintegration process of M-skin from a multi-foot origami robot. (E) The disintegration rates of M-skin over time when the gluten content changes from 0 to 10%. (F) The swelling times of M-skin increase as the environmental pH changes from 1 to 13. (G) M-skin disintegration rates over time under the same oscillating magnetic field (10 mT, 1 Hz) and diverse environmental pH (from 1 to 13). Error bars indicate the SD for $n = 3$.

M-skin and PVA can endow an M-skin with better film-forming ability and adhesiveness, both a lower mass fraction of gluten and a lower concentration of PVA solution will accelerate disintegration (Fig. 5E and fig. S12C). For instance, an M-skin without gluten can be disintegrated completely under the magnetic oscillation within 2 min, whereas an M-skin with 10% gluten can remain more than half intact after 4 min under disintegration conditions. Similarly, the M-skin adopting a 10% PVA solution concentration can be disintegrated in about 4 min, whereas the one adopting a 20% concentration of PVA solution disintegrated 20% in the same time. However, it is worth noting that the mass fraction of gluten and the concentration of PVA solution should be kept in a proper value in real practice, i.e., PVA solution concentration of ~10% and gluten of ~5%, by weighing the fabrication, adhesiveness, actuation, and reliability of M-skin. More details about the influence of each component to the M-skin is given in the Supplementary Materials.

Regarding the effect of pH value, the swelling and disintegrating process of M-skin will be accelerated as the acidity is enhanced because the weak hydrogen bonds between PVA chains will be re-

placed by the strong hydrogen bonds between PVA chains and hydrogen ions (Fig. 5, F and G, and tables S2 and S3). Specifically, the M-skin will start to disintegrate in about 8 min under the strong acid environment (pH 1) even without magnetic oscillation, caused by the chemical reaction between iron particles inside the M-skin and the hydrogen ions inside the acid (fig. S14, A and B). To prolong the effective working time of M-skin in the strong acid environment, two kinds of improvements can be adopted: One is coating an additional PVA layer on the surface of M-skin after curing, and another is changing the MPs into others that do not react with the hydrogen ions inside the acid, such as nickel. As the experimental results show in fig. S14 (C and D), the additional PVA covering can extend the disintegration without magnetic oscillation from ~8 to ~15 min, whereas the M-skin with nickel particles can keep stable in the strong acid environment even after 30 min.

M-skin-covered catheter for on-demand active navigating

The catheter is a widely used tool to treat diseases or to perform surgical procedures in the body cavity, duct, or vessel. Because of its

thin and flexible structure, the insertion is usually conducted passively, and the corner crossing is very challenging in practice. Here, we construct an M-skin catheter with active steering and navigating abilities by coating M-spray (thickness, $\sim 150\ \mu\text{m}$; length, 8 mm) on the existing flexible catheter head end (diameter, 1 mm) followed by an axial magnetization (Fig. 6A). In this design, the M-spray mainly plays two functions: One is to provide the magnetic force F to pull the flexible wire forward, and the other is to steer the course by magnetic torque T . Same as existing magnetic steering catheters (30–32), the bending radius r and degree θ of the tip depend on the ratio of flexible length L_{Flex} and stiff length L_{Stiff} , as well as the strength and direction of applied magnetic field. By leveraging an appropriate constraint and magnetic field, the constructed M-skin catheter can perform sharp or smooth turns.

To demonstrate the active guidance ability of the M-skin catheter, we conducted the targeting of the thrombus in a narrow blood vessel model (minimum diameter, 4 mm and maximum diameter,

9 mm) with a 120° branch corner. As illustrated in Fig. 6B, the constructed M-skin catheter first moves forward $\sim 45\ \text{mm}$ to the fork of blood vessels in 20 s by manual feeding and magnetic pulling. After that, we steer the direction of magnetic torque (rotate 60° clockwise) to make the catheter turn right about 60° into the target branch. Last, the catheter transports forward $\sim 30\ \text{mm}$ in 60 s to approach the target (movie S6). Considering the blood flow in practical vessels, we further investigated the motion ability and stability of an M-skin catheter under the effects of liquid flow (Supplementary Text). First, the impact of still blood itself on the disintegration is negligible, and the M-skin of the catheter can keep stable even after 2 hours (fig. S15A). The moving speed of catheter decreased as the liquid flow velocity increased (fig. S15D), but the influence of the blood flow on locomotion would not be a major issue because manual wire feeding is always used in clinical applications. For disintegration without the oscillating magnetic field, the M-skin was stable for 50 to 20 min as the liquid flow velocity changed from 50 to 200 mm/s (fig. S15E),

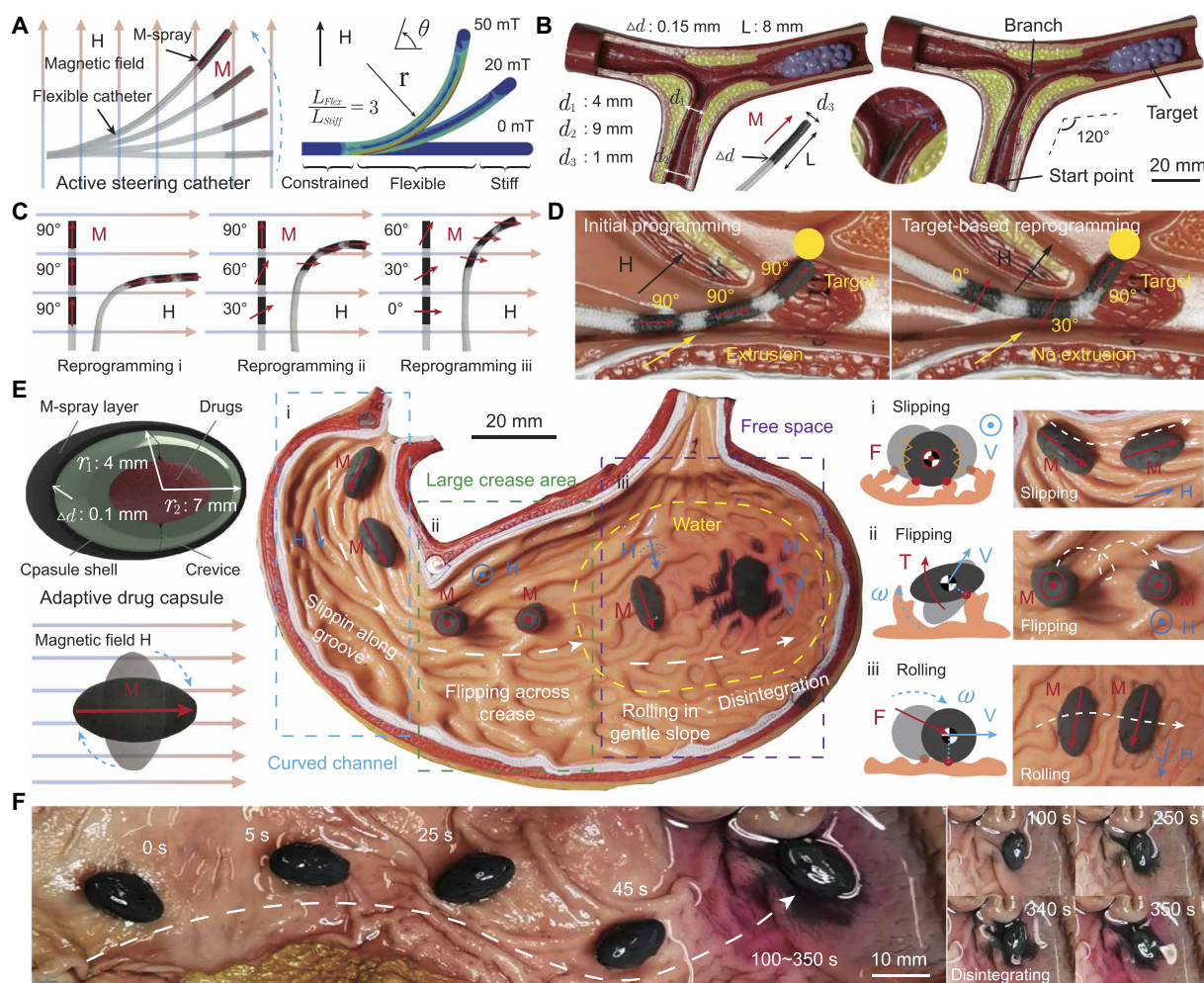


Fig. 6. Demonstrations and applications of M-skin millirobot. (A) Active steering catheter constructed by M-spray coating and its deformation model under magnetic fields with different strengths. (B) The navigation ability of the one-point catheter in the narrow vascular model. (C) The reprogramming of multi-point sampling cotton thread for various sets of steering. (D) Reprogramming the easy magnetization axis of multi-point sampling cotton thread according to the corner angle of the throat, which can achieve the fast directional steering under the actuation of magnetic torque and can reduce the risk of extrusion with throat wall during insertion. (E) The construction of an adaptive drug capsule millirobot and its multiple locomotion modes as well as controllable disintegration. (F) The controllable locomotion and disintegration of a constructed M-skin capsule for active delivery in an ex vivo animal model.

which is an acceptable value to meet the requirement of many clinical application cases.

Benefiting from the features of on-demand fabrication and reprogramming, our method can also set more than one coating region to construct the multi-point M-skin catheter flexibly. Different from the conventional magnetic steering catheter whose turning radius depends on the length of flexible section and the constraints from inner walls of working space, the multi-point M-skin catheter can achieve various sets of steering by programming the easy magnetization axis of each coating section (Fig. 6C), leading to higher adaptability in implementing tasks in harsh environments. Taking a multi-point M-skin sampling cotton thread as an example (Supplementary Text), to better fit the irregular corner structure of a throat with sharp turn of $\sim 90^\circ$ and a narrow radius of ~ 10 mm, we reprogrammed the thread accordingly to angles of 90° , 30° , and 0° for the three sections, respectively. As the results show in Fig. 6D, the target-based reprogrammed cotton thread can achieve the fast directional steering under the action of magnetic torque and can reduce the risk of extrusion with throat wall during insertion as well. The ability to quickly set the desired orientation and designed configuration without changing the main structure of the catheter offers promising potentials for catheter manipulation in the complex esophagus, vessel, and urethra, where navigation is always required.

M-skin-covered capsule for active delivery

An active drug delivery system demonstrates many advantages in disease treatment over traditional pills because of its higher local drug concentration and enhanced retention in the gastric mucous layer (33). Effective transportation of cargo containing drugs in multiple environments (dry, wet, flat, and pleated surface) would promote clinical applications. For instance, the stomach is relatively “dry” when empty but will become “wet” when full of food, water, and gastric juice. Moreover, if the lesion (e.g., stomach ulcer) is at the top of the stomach where liquid media cannot reach it easily due to gravity, a robot that can work at such environment could help. Compared with existing drug delivery systems (33–35), which are usually designed to work in liquid media (gastric juice and blood), our M-skin millirobot could achieve effective locomotion on different surfaces and in different media. That makes it a useful tool for the task in complex cavities, such as esophagus, stomach, and intestine. Moreover, the controllable disintegration property of the covered M-skin endows existing pills with an ability to release on demand, for instance, only releasing in the infection region rather than scattering randomly in the whole organ.

To demonstrate the adaptive locomotion and controllable drug releasing ability, we converted a nondeformable ellipsoidal capsule to an M-skin millirobot by coating it with M-spray. The capsule shell was cut into two halves and agglutinated with M-spray to achieve controllable drug release by disintegrating the M-skin. As illustrated in Fig. 6E, the constructed adaptive drug capsule contains three layers in total, i.e., M-skin cover (thickness, ~ 100 μm), middle capsule shell (short axis, 8 mm; long axis, 14 mm), and the internal drugs (dyed by red stain Rhodamin 6G for visualization). Under the actuation of magnetic field, the constructed M-skin capsule was able to locomote at different modes—including slipping, flipping, and rolling—corresponding to the environment. For instance, the M-skin capsule could swing with a small amplitude of ~ 3 mm to decrease the friction from the ground, reach a motion speed of ~ 1 mm/s by adopting the longitudinal slipping motion

along the groove of creases in the narrow curved channel (locomotion type i), flip across the staggered creases with a ~ 5 times higher speed than slipping in the large crease area (locomotion type ii), and roll with a ~ 10 times higher speed than slipping on the relatively open and flat space (locomotion type iii). Even challenged by the slippery surface and viscous resistance of the ropy gastric juice, the locomotion of M-skin capsule was still controllable and efficient (Fig. 6F). After reaching the target lesion, by applying the oscillating magnetic field (10 mT, 1 Hz), the connection between two halves of the capsule became unstable, and the drug (red stain) began to seep through the crevice (movie S7).

In vivo demonstration in rabbit stomach model

To further verify the feasibility and effectiveness of an M-spray-enabled millirobot for biomedical applications, we conducted an in vivo drug delivery test in the rabbit stomach using the M-skin capsule. As illustrated in Fig. 7A, we set the targeted region at the end of the stomach and close to the intestine. To demonstrate the drug delivery both in vivo (ultrasound imaging) and in vitro (cutting open stomach), we encapsulated microglass beads (500 μm) and biological stain (Indigo carmine, Phygene Scientific, PH9195) into the capsule. During the experiment, we orally administered 1.0-g beads for control group 1 and 0.05-g biological stain for control group 2, whereas the M-skin capsule contained 1.0-g beads for experiment group 1 and 0.05-g biological stain for experiment group 2. These four rabbit groups underwent 8 hours of fasting treatment before the experiment, and water feeding and anesthesia were kept during the whole experiment process (Materials and Methods).

Owing to the covering of M-skin, the capsule in the stomach can be detected by radiology imaging [digital subtraction angiography (DSA), CGO-2100, Wandong], the position and orientation of which can then be used as a feedback for the robot actuation by magnetic field. As the time-lapse radiology images (from experiment group 1) in Fig. 7B show, the constructed M-skin capsule tolerated the ropy and the acid environment and achieved controllable locomotion with an “O” trajectory in the stomach. When the M-skin capsule approached the designed targeted region, the M-skin was disintegrated by applying the oscillating magnetic field to controllably release the encapsulated beads and stain. Figure 7C gives the in vivo comparison results of the microbead release by ultrasound imaging. It indicates that the M-skin capsule can concentrate the beads’ release on the targeted region, i.e., the bright region on the stomach wall, whereas the distribution of beads was almost sparse and could be hardly detected in control group 1. To further intuitively demonstrate the targeted diffusion and retention of drug, we replaced the beads by biological stain and repeated the control experiment with the same process. Then, the rabbits were euthanized, and their stomachs were collected to observe the distribution of biological stain after half an hour. As illustrated in Fig. 7D, comparing with the unintended diffusion in control group 2, the active drug delivery of M-skin capsule in experiment group 2 could effectively enhance the retention and the concentration of drug in specific lesions (~ 150 mm^2). These results suggest that the constructed M-skin capsule is feasible and effective for in vivo drug delivery.

DISCUSSION

Constructing a robot that can effectively adapt to different environments and interact with diverse objects is a grand challenge in

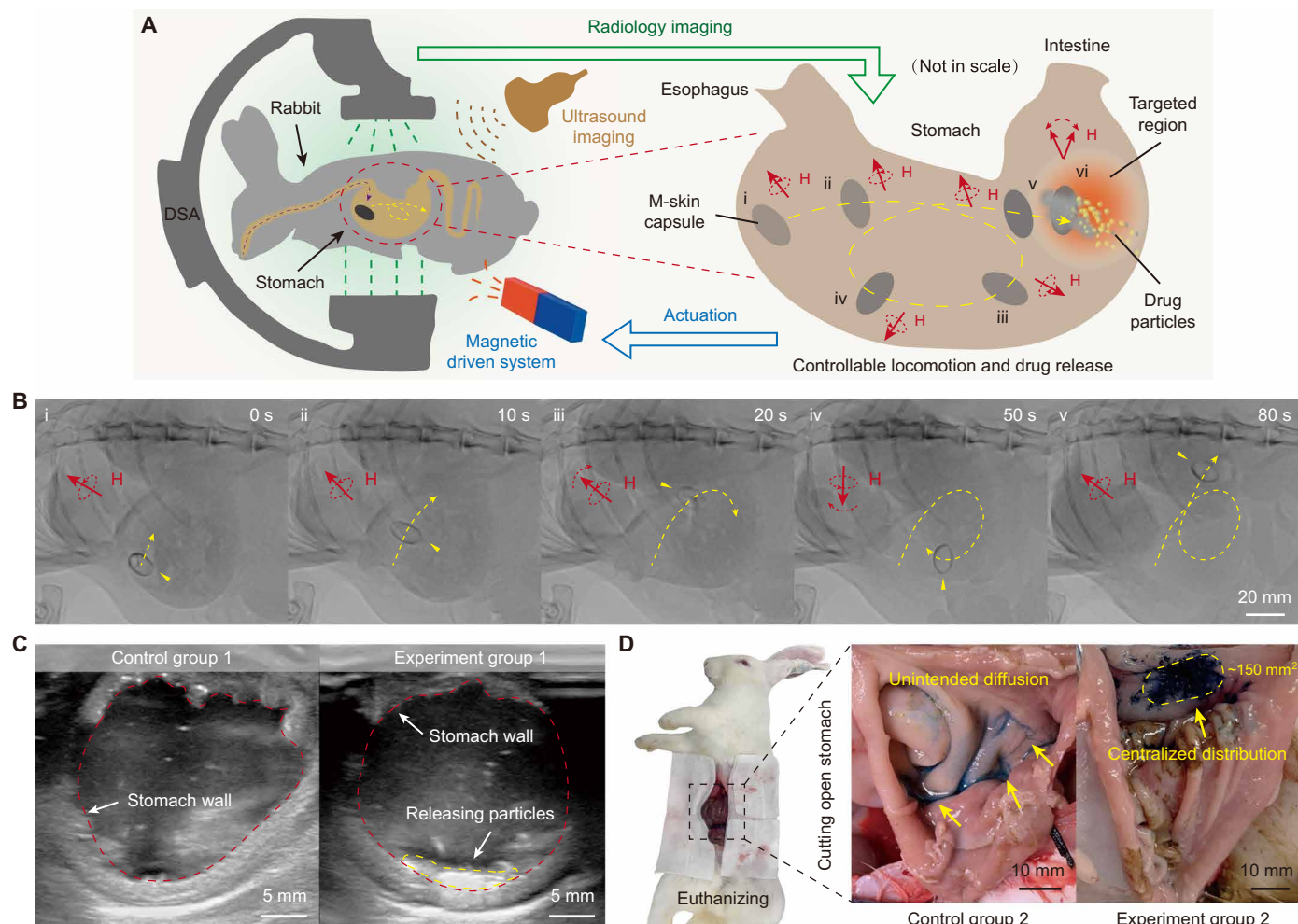


Fig. 7. In vivo demonstration in rabbit stomach model. (A) Schematic of the drug delivery in rabbit stomach. The magnetic field is applied for robot actuation, radiology imaging is adopted for locomotion evaluation, and ultrasound imaging is adopted for drug release evaluation. (B) Radiology images of an M-skin capsule steered in a stomach with a controllable O trajectory. (C) Ultrasound images for the in vivo evaluation of bead diffusion. The distribution of beads is sparse with limited detection in control group 1, whereas the bright region on the stomach wall in experiment group 1 indicates that the M-skin capsule can concentrate bead release on the targeted region. (D) Optical images showing the retention of biological stain in control group 2 (left) and experiment group 2 (right).

robotics. Considering that target objects usually vary from each other in size, shape, and structure, it is challenging to develop an end effector or robot to handle all cases. Moreover, for the tasks in limited space, e.g., object transportation, the acceptable size increment superposed to the target is strictly limited, which raises higher demand for the robot design at small scale.

We exploit a simple fabrication process for on-demand millirobots. Our approach leverages the adhesiveness and wetting ability of M-spray to turn a variety of milli-objects into millirobots regardless of the surface condition, e.g., flat or curve and hydrophilic or hydrophobic. Because the M-skin only accounts for a small volume ratio, it is able to preserve the original size, morphology, and structure of covered objects. Because the structure of an inanimate target is fully used for locomotion, the constructed robot demonstrates high working efficacy and loading ability, which can reach up to thousandfold of its own volume and hundredfold of its own weight. Moreover, our millirobots are also reprogrammable and can demonstrate multimodal locomotion, thus enabling our robots to

better adapt to various environments. Note that the M-spray is unharmed to the host owing to its disintegrable properties. The strategy of turning inanimate objects into moveable millirobots on demand can quickly realize the effective object operation, offering potentials for manipulation, transportation, and delivery in unpredictable, limited spaces.

MATERIALS AND METHODS

Raw materials of M-spray

The PVA with 87.0 to 89.0% degree of alcoholysis was bought from Aladdin Chemistry Co. Ltd. Gluten (wheat protein) was obtained from Mingzuotang fishing tackle Corporation. Iron micropowder [Spherical, aerodynamic particle sizer (APS) 6 to 10 μm , reduced, 99.5%] was purchased from Alfa Aesar. Water with a resistivity of 18.2 megohms-cm at 25°C was acquired from a Millipore Milli-Q system and was used for all solution preparations. The 10 wt % PVA solution was prepared under stirring at 500 rpm for 2 hours under 90°C with a magnetic

stirrer (RCT basic, German IKA Corporation). Then, the raw material of the M-spray was obtained by mixing gluten and iron powder with 10% PVA solution at a mass ratio of 1:8:11 by stirring for several minutes. All chemicals with the purity of analytical reagent grade were used as received without further purification.

The magnetization characterization of M-skin

The magnetization (magnetic moment density) of M-skin with different magnetic field strengths and MP mass fractions was measured by a vibrating sample magnetometer (DMS 1660, ADE Technologies). Here, the peeled M-skin sample size was 10 mm by 10 mm with thickness of ~0.2 mm. As the result shows in Fig. 1E, when we kept the MP mass fraction within 40%, the magnetization of M-skin increased from 0 to 166.1 kA/m as the applied magnetic field changed from 0 to 200 mT. As shown in Fig. 1F, when we maintained the applied magnetic field at 100 mT and adjusted the MP mass fraction from 30 to 50%, the measured magnetization increased from 72.2 to 154.9 kA/m correspondingly.

The peeling strength test of M-spray to different materials

The combining force between the M-spray and inanimate objects was evaluated by the peeling strength. In the test, the M-spray was daubed as a strip (25 mm by 50 mm) on the surface of different testing objects, including standard A4 paper (Double A, premium), wood (Cedar), PDMS (0.1 equivalent curing agents, Sylgard 184, Dow Corning), glass slide (catalog no. 7107, Sail brand), and plastic sheet (polyethylene). After the evaporation of excess water, we peeled the cured M-spray along the long axis direction with a constant speed of 2.5 mm/s. The dynamometer (ELK-20, 0.01 N precision, Elecall Corporation) was used to obtain the average force during the peeling process.

The fabrication process of the M-skin millirobots

In general, the fabrication of the M-skin millirobot followed the same coating, magnetizing, and curing process. For the fully coated walking robot (fig. S6A), we first coated the M-spray on the curved PDMS film and then stretched it to a plane and magnetize (100 mT) along the long axis during the curing process. After curing, we could obtain the walking robot by recovering the PDMS film to curve. For the soft reptile robot and rolling robot, which were partly coated (fig. S6, C and D), we used a mask to protect the unselected region before coating M-spray. Then, the magnetic field with a strength of 100 mT was adopted to magnetize the robot with a single magnetization direction during curing. Last, the designed reptile robot and rolling robot could be obtained after curing. The multi-foot origami robot (fig. S6B) was constructed with multiple partial coats and with multiple magnetization directions. First, we printed the designed pattern on the paper as the substrate of the constructed origami robot. Second, the mask with a designed penetrable area was used to select the first coating region. After the spraying, magnetizing, and curing, we obtained the first coating region. Then, we selected other regions with the mask and repeated the spraying, the magnetizing, and curing. Last, we obtained the magnetic multi-foot origami robot by cutting and folding the substrate.

Disintegration evaluation of M-skin

The cured M-skin in still water could maintain stability but become disintegrable after applying magnetic agitation generated by the Helmholtz coil system. Here, the disintegration rate was defined as

the ratio between the area of fragmentation and the original area of M-skin. Fragmentations with a size smaller than 2.5% of the origin area were considered as disintegrated. For the disintegration analysis of free M-skin, the size of M-skin was 5 mm by 5 mm, and the applied magnetic field had a strength of 10 mT and frequency from 0 to 5 Hz. To investigate the influences of different substrate surfaces on the M-skin disintegration, the M-spray with the same size of 5 mm by 5 mm was daubed to the different material substrates (table S4) under an applied magnetic field with a strength of 10 mT and a frequency of 1 Hz.

In vivo experiment setup

This study aims to collect basic evidence for drug delivery function of the proposed millirobot in live animals. Four 8- to 12-week-old male New Zealand rabbits, weighing 1.8 to 2.1 kg, were obtained from Shenzhen Advanced Medical Services Co. Ltd. and randomly divided into four groups. No animal was excluded from this study. All rabbits underwent 8 hours of fasting treatment before the experiment. Both water feeding and anesthesia were maintained during the whole experiment process. Experiment group 1 was treated by oral administration of the constructed M-skin capsules containing 1.0-g glass bead particles (500 μ m), and the same glass beads without M-skin capsules were orally delivered to control group 1. Experiment 2 was treated by the constructed M-skin capsules containing 0.05-g biological stain (Indigo carmine, Phygene Scientific, PH9195), and control group 2 was given the same amount of stain without M-skin capsules by oral delivery. The locomotion of M-skin capsule was achieved by magnetic field, and its position was detected by radiology imaging (DSA, CGO-2100, Wandong). Because of the harmfulness of radiology imaging, the magnetic actuation and imaging were conducted at intervals. After half an hour, the retention of glass beads in vivo (control group 1 and experiment group 1) was evaluated by ultrasound imaging (Philips EPIQ 7 ultrasound system), and the diffusion of biological stain (control group 2 and experiment group 2) was observed by collecting the stomachs after euthanasia.

SUPPLEMENTARY MATERIALS

robotics.sciencemag.org/cgi/content/full/5/48/eabc8191/DC1

Supplementary Text

Fig. S1. The comparison of adhesion property between water droplet and M-spray droplet.

Fig. S2. The curing process and magnetic property of M-spray and the equipment used for magnetic field production.

Fig. S3. Actuating performance of the M-skin under magnetic field.

Fig. S4. Mechanical properties and adhesiveness of the cured M-spray.

Fig. S5. The design and locomotion analysis of diverse M-skin millirobots.

Fig. S6. The construction process of M-skin millirobots.

Fig. S7. The actuation of M-skin millirobots by permanent magnet.

Fig. S8. Locomotion demonstration of the constructed M-skin millirobots.

Fig. S9. The performance evaluation of different motion modes on diverse surfaces.

Fig. S10. The environment adaptability and obstacle overcoming ability of diverse M-skin millirobots.

Fig. S11. The constructed M-skin millirobots work in both land and liquid environment.

Fig. S12. Controllable magnetic-induced disintegration of M-skin in aquatic environment.

Fig. S13. The process that M-skin detaches after task completing from target inanimate objects.

Fig. S14. The disintegration of M-skin with different material components in strong acid environment (pH 1) without magnetic oscillation.

Fig. S15. The influence of physiological blood flow on the locomotion speed and disintegration process of M-skin catheter.

Table S1. The performance evaluation summary of different motion modes under diverse surface conditions.

Table S2. The swelling and disintegration of M-skin without magnetic oscillation under different environmental temperature and pH.

Table S3. The swelling and disintegration time of cured film composed of different materials without magnetic oscillation.

Table S4. Substrates used in the M-skin disintegration testing.

Movie S1. Coating of the M-spray droplet on target surfaces.

Movie S2. M-spray-enabled M-skin millirobots.

Movie S3. The environment adaptability of constructed M-skin millirobots.

Movie S4. Topology order reprogramming of the M-skin millirobot.

Movie S5. Magnetic-induced disintegration.

Movie S6. M-skin-covered catheter for active navigating.

Movie S7. M-skin-covered capsule for target drug delivery.

References (36, 37)

REFERENCES AND NOTES

- Z. Zhakypov, K. Mori, K. Hosoda, J. Paik, Designing minimal and scalable insect-inspired multi-locomotion millirobots. *Nature* **571**, 381–386 (2019).
- M. Sitti, Miniature soft robots—Road to the clinic. *Na. Rev. Mater.* **3**, 74–75 (2018).
- K. Y. Ma, P. Chirarattananon, S. B. Fuller, R. J. Wood, Controlled flight of a biologically inspired, insect-scale robot. *Science* **340**, 603–607 (2013).
- X. Ji, X. Liu, V. Caccucio, M. Imboden, Y. Civet, A. El Haitami, S. Cantin, Y. Perriard, H. Shea, An autonomous untethered fast soft robotic insect driven by low-voltage dielectric elastomer actuators. *Sci. Robot.* **4**, (2019).
- M. Cianchetti, C. Laschi, A. Menciasci, P. Dario, Biomedical applications of soft robotics. *Nat. Rev. Mater.* **3**, 143–153 (2018).
- H. Xie, M. Sun, X. Fan, Z. Lin, W. Chen, L. Wang, L. Dong, Q. He, Reconfigurable magnetic microrobot swarm: Multimode transformation, locomotion, and manipulation. *Sci. Robot.* **4**, eaav8006 (2019).
- Y. Chen, H. Zhao, J. Mao, P. Chirarattananon, E. F. Helbling, N. S. P. Hyun, D. R. Clarke, R. J. Wood, Controlled flight of a microrobot powered by soft artificial muscles. *Nature* **575**, 324–329 (2019).
- M. Lahikainen, H. Zeng, A. Priimagi, Reconfigurable photoactuator through synergistic use of photochemical and photothermal effects. *Nat. Commun.* **9**, 1–8 (2018).
- A. Lendlein, Fabrication of reprogrammable shape-memory polymer actuators for robotics. *Sci. Robot.* **3**, (2018).
- W. Hu, G. Z. Lum, M. Mastrangeli, M. Sitti, Small-scale soft-bodied robot with multimodal locomotion. *Nature* **554**, 81–85 (2018).
- H. Lu, M. Zhang, Y. Yang, Q. Huang, T. Fukuda, Z. Wang, Y. Shen, A bioinspired multilegged soft millirobot that functions in both dry and wet conditions. *Nat. Commun.* **9**, 1–7 (2018).
- S. Tottori, L. Zhang, F. Qiu, K. K. Krawczyk, A. Franco-Obregón, B. J. Nelson, Magnetic helical micromachines: Fabrication, controlled swimming, and cargo transport. *Adv. Mater.* **24**, 811–816 (2012).
- S. D. de Rivaz, B. Goldberg, N. Doshi, K. Jayaram, J. Zhou, R. J. Wood, Inverted and vertical climbing of a quadrupedal microrobot using electroadhesion. *Sci. Robot.* **3**, eaau3038 (2018).
- Y. Wu, J. K. Yim, J. Liang, Z. Shao, M. Qi, J. Zhong, Z. Luo, X. Yan, M. Zhang, X. Wang, R. S. Fearing, Insect-scale fast moving and ultrarobust soft robot. *Sci. Robot.* **4**, eaax1594 (2019).
- Y. Zhang, B. K. Chen, X. Liu, Y. Sun, Autonomous robotic pick-and-place of microobjects. *IEEE Trans. Robot.* **26**, 200–207 (2009).
- J. Hughes, U. Culha, F. Giardina, F. Guenther, A. Rosendo, F. Iida, Soft manipulators and grippers: A review. *Front. Robot. AI* **3**, 69 (2016).
- Z. Ren, W. Hu, X. Dong, M. Sitti, Multi-functional soft-bodied jellyfish-like swimming. *Nat. Commun.* **10**, 1–12 (2019).
- H. Gu, Q. Boehler, H. Cui, E. Secchi, G. Savorana, C. De Marco, S. Gervasoni, Q. Peyron, T. Y. Huang, S. Pane, A. M. Hirt, Magnetic cilia carpets with programmable metachronal waves. *Nat. Commun.* **11**, 1–10 (2020).
- H. W. Huang, F. E. Uslu, P. Katsamba, E. Lauga, M. S. Sakar, B. J. Nelson, Adaptive locomotion of artificial microswimmers. *Sci. Adv.* **5**, eaau1532 (2019).
- X. Chen, H. Yuk, J. Wu, C. S. Nabzdyk, X. Zhao, Instant tough bioadhesive with triggerable benign detachment. *Proc. Natl. Acad. Sci. U.S.A.* **117**, 15497–15503 (2020).
- S. Saito, S. Nobusue, E. Tsuzaka, C. Yuan, C. Mori, M. Hara, T. Seki, C. Camacho, S. Irlle, S. Yamaguchi, Light-melt adhesive based on dynamic carbon frameworks in a columnar liquid-crystal phase. *Nat. Commun.* **7**, 12094 (2016).
- G. Ju, M. Cheng, F. Guo, Q. Zhang, F. Shi, Elasticity-dependent fast underwater adhesion demonstrated by macroscopic supramolecular assembly. *Angew. Chem. Int. Ed.* **57**, 8963–8967 (2018).
- F. W. DelRio, M. P. de Boer, J. A. Knapp, E. D. Reedy, P. J. Clews, M. L. Dunn, The role of van der Waals forces in adhesion of micromachined surfaces. *Nat. Mater.* **4**, 629–634 (2005).
- R. Hodge, G. H. Edward, G. P. Simon, Water absorption and states of water in semicrystalline poly(vinyl alcohol) films. *Polymer* **37**, 1371–1376 (1996).
- S. D'Amico, M. Hrabalova, U. Müller, E. Berghofer, Bonding of spruce wood with wheat flour glue—Effect of press temperature on the adhesive bond strength. *Ind. Crops Prod.* **31**, 255–260 (2010).
- Y. Kim, H. Yuk, R. Zhao, S. A. Chester, X. Zhao, Printing ferromagnetic domains for untethered fast-transforming soft materials. *Nature* **558**, 274–279 (2018).
- W. Wang, J. Y. Lee, H. Rodrigue, S. H. Song, W. S. Chu, S. H. Ahn, Locomotion of inchworm-inspired robot made of smart soft composite (SSC). *Bioinspir. Biomim.* **9**, 046006 (2014).
- J. Kim, S. E. Chung, S. E. Choi, H. Lee, J. Kim, S. Kwon, Programming magnetic anisotropy in polymeric microactuators. *Nat. Mater.* **10**, 747–752 (2011).
- H. Markides, M. Rotherham, A. El Haj, Biocompatibility and toxicity of magnetic nanoparticles in regenerative medicine. *J. Nanomater.* **2012**, 1–11 (2012).
- Y. Kim, G. A. Parada, S. Liu, X. Zhao, Ferromagnetic soft continuum robots. *Sci. Robot.* **4**, eaax7329 (2019).
- V. N. Le, N. H. Nguyen, K. Alameh, R. Weerasooriya, P. Pratten, Accurate modeling and positioning of a magnetically controlled catheter tip. *Med. Phys.* **43**, 650–663 (2016).
- C. Chautems, A. Tonazzini, Q. Boehler, S. H. Jeong, D. Floreano, B. J. Nelson, Magnetic continuum device with variable stiffness for minimally invasive surgery. *Adv. Intelligent Syst.* **2**, 1900086 (2020).
- B. E. F. de Avila, P. Angsantikul, J. Li, M. A. Lopez-Ramirez, D. E. Ramirez-Herrera, S. Thamphiwatana, C. Chen, J. Delezuk, R. Samakapiruk, V. Ramez, M. Obonyo, Micromotor-enabled active drug delivery for in vivo treatment of stomach infection. *Nat. Commun.* **8**, 1–9 (2017).
- Y. Alapan, U. Bozuyuk, P. Erkoc, A. C. Karacakol, M. Sitti, Multifunctional surface microrollers for targeted cargo delivery in physiological blood flow. *Sci. Robot.* **5**, eaba5726 (2020).
- K. Villa, L. Krejčová, F. Novotný, Z. Heger, Z. Sofer, M. Pumera, Cooperative multifunctional self-propelled paramagnetic microrobots with chemical handles for cell manipulation and drug delivery. *Adv. Funct. Mater.* **28**, 1804343 (2018).
- P. Pappas, The original Ampère force and Biot-Savart and Lorentz forces. *Il Nuovo Cimento B (1971–1996)* **76**, 189–197 (1983).
- E. J. Haug, S. C. Wu, S. M. Yang, Dynamics of mechanical systems with Coulomb friction, stiction, impact and constraint addition-deletion—I theory. *Mech. Mach. Theory* **21**, 401–406 (1986).

Funding: This work was supported by the National Science Foundation of China (61773326 and U1813211) and Hong Kong RGC General Research Fund CityU 11214817. **Author contributions:** X.Y. and W.S. contributed equally to this work. X.Y. designed the robot and carried out the experiments. W.S. and X.W. developed the robot model. H.L. contributed to scientific discussion and experiment design. Y.L. and R.T. carried out the experiment in material synthesis. L.Y. designed the animal experiment and processed the data. Y.S. conceived the idea and led the project. **Competing interests:** The authors declare that they have no competing interests. **Data and materials availability:** All data needed to evaluate the conclusions in the paper are present in the paper and/or the Supplementary Materials. Additional data related to this paper may be requested from the authors.

Submitted 15 May 2020

Accepted 26 October 2020

Published 18 November 2020

10.1126/scirobotics.abc8191

Citation: X. Yang, W. Shang, H. Lu, Y. Liu, L. Yang, R. Tan, X. Wu, Y. Shen, An agglutinate magnetic spray transforms inanimate objects into millirobots for biomedical applications. *Sci. Robot.* **5**, eabc8191 (2020).

An agglutinate magnetic spray transforms inanimate objects into millirobots for biomedical applications

Xiong YangWanfeng ShangHaojian LuYanting LiuLiu YangRong TanXinyu WuYajing Shen

Sci. Robot., 5 (48), eabc8191. • DOI: 10.1126/scirobotics.abc8191

View the article online

<https://www.science.org/doi/10.1126/scirobotics.abc8191>

Permissions

<https://www.science.org/help/reprints-and-permissions>

Use of this article is subject to the [Terms of service](#)